THESIS

EVALUATING THE EFFECT DYNEIN AND RELATED PROTEINS EXHIBIT ON THE SPINDLE ASSEMBLY CHECKPOINT AND KINETOCHORE.

Submitted by

Tyler Biebighauser

Department of Biochemistry and Molecular Biology

In partial fulfillment of the requirements

For the Degree of Master of Science

Colorado State University

Fort Collins, Colorado

Summer 2019

Master's Committee:

Advisor: Steven Markus

Co-Advisor: Jennifer DeLuca

Santiago Di Pietro

Fred Hoerndli

ABSTRACT

EVALUATING THE EFFECT DYNEIN AND RELATED PROTEINS EXHIBIT ON THE SPINDLE ASSEMBLY CHECKPOINT AND KINETOCHORE

To ensure that cell division is faithfully carried out without causing genetic errors, eukaryotic cells have evolved several conserved checkpoints during mitosis. One such checkpoint, the Spindle Assembly Checkpoint (SAC), blocks the cell from progressing through metaphase until all chromosomes have become bi-oriented by microtubules. Only once this occurs can the cell progress into anaphase to separate the sister chromatids. Errors in this checkpoint have been linked with aneuploidy, which itself is linked with oncogenesis. Naturally there are many layers of regulation within the SAC, most of which are associated with a proteinaceous structure on the sister chromatid – the kinetochore. The molecular motor dynein, and its kinetochore localized co-factors play several roles in this regulation. In one of these roles, dynein strips away kinetochore localized signal proteins upon microtubule bi-orientation, to weaken the strength of the SAC. We initially set out to test whether this process of SAC stripping has further levels of regulation, or if all dynein requires to strip these signal proteins is the presence of a microtubule. We used *in-vitro* motility assays to investigate whether dynein's motility along microtubules is changed depending on the length of its kinetochore localized cargo adapter, spindly. We purified truncated versions of spindly to test if it undergoes regulation analogous to other dynein cargo adapters. These *in-vitro* motility assays showed no difference in dynein motility past a certain length required to confer motility. Interestingly, we observed that some of the shorter spindly truncations undergo phase separation both *in-vitro* in the right conditions and *in-vivo* when transfected into HeLa cells. We postulate that this phase

separation could have implications in a process called fibrous corona expansion, which occurs on a kinetochore that has spent a long time in prometaphase without attaching to a microtubule. In total these studies shed light on the nature of interactions at the kinetochore, and the complexity of regulation as it pertains to dynein mediated kinetochore stripping.

TABLE OF CONTENTS

Introduction and Background

In order to properly undergo cell division, a metazoan cell must duplicate and segregate its chromosomes into two daughter cells. To begin, the cell duplicates its chromosomes during S phase of the cell cycle. When a cell enters mitosis, it enters in prophase, characterized by the condensation of chromatin and the breakdown of the nuclear envelope. After nuclear envelope breakdown, the cell enters prometaphase. During this stage, a proteinaceous structure on the chromosome called a kinetochore is formed. Also, a structure composed of microtubules and their associated proteins called the mitotic spindle forms. Within this spindle, microtubules will bind to kinetochores in preparation for metaphase and anaphase. In metazoan cells, there are two kinetochores per mitotic chromosome, one per sister chromatid. The cell enters metaphase when all kinetochores are bound to microtubules, and the microtubules align the chromosomes into a metaphase plate along the spindle equator. Upon activation of anaphase, the kinetochore-attached microtubules will depolymerize, taking a sister chromatid with it to one of the centrosomes. The cell culminates mitosis during telophase, in which a new nuclear envelope envelops the two resulting pools of DNA within the cell. Additionally, DNA will begin to de-condense. The cell will then undergo cytokinesis, a process which splits the cell into two, with each resulting cell typically receiving the same genetic information.

The Spindle Assembly Checkpoint

To establish an accurate segregation of chromosomes during mitosis, metazoan cells have developed a checkpoint to ensure that all kinetochores have been attached to microtubules before anaphase can occur. This checkpoint, called the Spindle Assembly Checkpoint (SAC) propagates a diffusible “anaphase wait” signal, keeping the cell in

metaphase until the last kinetochore has been attached to a microtubule (Heasley et al. 2017). It has been observed that even one unattached kinetochore will stall the progression of mitosis for the entire cell (Li and Nicklas 1995; Rieder et al. 1995). Kinetochore microtubule attachment is a dynamic process, with many erroneous attachments being made before correct, end-on attachments are made (Cimini et al. 2003; Magidson et al. 2011). Erroneous attachments include, among others, syntelic attachments, where both kinetochores on a chromosome are attached to the same spindle pole, and merotelic attachments, a single kinetochore is attached to microtubules from both spindle poles. Should anaphase occur while a kinetochore is improperly attached to microtubules, aneuploidy can occur, whereby the resulting daughter cells contain either too many or too few chromosomes. This genetic instability is strongly linked with oncogenesis (reviewed in Thompson et al. 2011). If too much time passes with improper kinetochore microtubule attachments, a phenomenon called cohesion fatigue will set in, which again could lead to chromosome instabilities (Daum et al. 2011; Stevens et al. 2011). Thus, the timing of when to silence the SAC is of great importance to ensure chromosome instability, and by extension oncogenesis, does not occur.

To progress from metaphase to anaphase, the Anaphase Promoting Complex/Cyclosome (APC/C), an E3 ubiquitin ligase, must be activated to facilitate the proteasomal degradation of important mitotic proteins such as cyclin B and Securin (King et al. 1995; Sudakin et al. 1995). An activator of the APC/C is the protein Cdc20, which presents targets to the APC/C (Visintin et al. 1997). The Mitotic Checkpoint Complex (MCC), which composes the “wait anaphase” signal, functions to sequester Cdc20 away from the APC/C, halting the progression of mitosis (Li et al. 1997; Fang et al. 1998). When a sufficient amount of kinetochore localized MCC is degraded or depleted, Cdc20 activates the APC and anaphase is initiated.

The Kinetochore

The kinetochore is made up of three domains: the inner kinetochore, the outer kinetochore, and the outer-most fibrous corona. The inner kinetochore is typically thought to be a scaffold of sorts, providing the foundation of the kinetochore, as well as recognizing and binding to specific sequences of DNA. The outer kinetochore contains proteins responsible for signaling, as well as proteins responsible for microtubule capture and attachment. KNL-1 is a protein found at the outer kinetochore that lays the groundwork for the recruitment of many of the SAC signal proteins. It is also involved in the recruitment of NDC-80, an important complex that promotes kinetochore-microtubule interactions, and has been implicated in the recruitment of the RZZ complex (Caldas et al. 2015; Cheeseman and Desai, 2008; DeLuca and Musacchio, 2012; Desai et al. 2003; Sarangapani and Asbury, 2014). The RZZ complex is made up of three proteins in a 2:2:2 stoichiometric ratio: Rough deal (ROD), Zeste White-10 (ZW10), and Zwilch (Gama et al. 2017; Mosalaganti et al. 2017). The RZZ complex accociates with kinetochores, whee it functions in part to recruit spindly, which in turn, recruits the molecular motor dynein to the kinetochore (Chan et al. 2009; Griffis et al. 2007). The outermost fibrous corona is made up of the RZZ complex, spindly and dynein, a subset of SAC proteins including Mad1 and Mad2, and the proteins CENP-E and CENP-F, which contribute to the capture of spindle microtubules. It has been observed that the fibrous corona undergos significant expansion if the kinetochore spends an extended amount of time unattached to microtubules (Magidson et al. 2015). In addition to increasing the number of molecules perpetuating the “wait anaphase” signal (i.e SAC proteins), it is thought that the expansion of the fibrous corona creates a larger platform for microtubule capture. Recently, several papers have suggested that the RZZ complex, along with spindly and dynein is the driving force behind this expansion (Pereira et al. 2018; Rodriguez-Rodriguez et al. 2018; Sacristan et al. 2018).

Dynein

Dynein is a minus end directed microtubule motor protein responsible for not only all retrograde traffic in a human cell, but also for many other functions, particularly in mitosis. Dynein binds to microtubules via its microtubule binding domain. The registry of the microtubule binding domain confers structural information distal to the microtubule through a coiled-coil stalk to a AAA ATPase domain responsible for the hydrolysis of ATP to confer mechanical work. Even more distal than the AAA ATPase is the N-terminal tail, which contains various binding sites for smaller dynein chains and a cargo adapter. Additionally, the tail also contains a dimerization domain such that two dynein monomers will form a dimer.

Metazoan dynein will not walk along microtubules on its own, rather, it must be in complex with a 23 subunit, 1.2 MDa complex named dynactin (for dynein activator) (McKenney et al. 2014; Schlager et al. 2014; Urnavicious et al. 2015). Dynactin is thought to position the dynein heads in an orientation conducive to walking along microtubules. However, the complex has a low affinity for dynein, so a cargo adapter facilitates the interaction between dynein and dynactin, in addition to binding to the cargo to be trafficked (McKenney et al. 2014; Schlager et al. 2014; Splinter et al. 2012).

Dynein cargo adapters have previously been shown to confer regulation on dynein/dynactin. For example, the best studied cargo adapter, Bicaudal D homolog 2 (BicD2), has been shown to fold back on itself in an auto-inhibitory manner. Upon binding to cargo, it unfolds, thereby opening and unmasking the binding sites for dynein and dynactin (Hoogenraad et al. 2003; Sladewski et al. 2018). This auto-inhibition helps to ensure that dynein is not active and needlessly exhausting ATP when not bound to any cargo.

Dynein Activated SAC Stripping

There are several ways kinetochore levels of MCC can be reduced to promote progression through metaphase. One such way is dynein-mediated. Upon attachment of a microtubule to a kinetochore, kinetochore localized dynein will carry various proteins, including a component of the MCC, Mad2, from the kinetochore to the centrosome. In stripping Mad2 and other proteins from the kinetochore, dynein removes an inhibitor of the APC from the kinetochore to further progress mitosis.

Dynein's kinetochore localized cargo adapter, spindly, is required for SAC silencing, presumably for its ability to help confer dynein motility (Griffis et al. 2007; McKenney et al. 2014; Schlager et al. 2014). Human spindly is a cell cycle regulated, 605 amino acid protein (Barisic et al. 2010). It is predicted to be a coiled coil, like all other dynein effectors whose atomic structures have been solved. (Kelley et al. 2015; Urnavicius et al. 2015). Spindly seems to have little conservation with other dynein effectors, however some dynein effectors do share a short "spindly motif" that is essential for conferring motility to the dynein complex (Gama et al. 2017; Gassmann et al. 2010). Previous small angle x-ray scattering data suggests one half of the spindly coiled-coil folds back to bind to the other (Sacristan et al. 2018). It appears this folding back inhibits spindly's natural ability to oligomerize, and it is hypothesized that this oligomerization is responsible for the expansion of the fibrous corona (Pereira et al. 2018; Rodriguez-Rodriguez et al. 2018; Sacristan et al. 2018).

To delve further into the regulation of the spindle assembly checkpoint, and corona expansion during prometaphase, we purified several truncations of spindly, and in doing so, discovered several spindly truncations that displayed characteristics of phase separation.

Results

We initially set out to test whether spindly undergoes auto-inhibition, and if this auto-inhibition is responsible for regulating the motility of the dynein apparatus as it relates to SAC stripping. Motility is defined as the ability of a molecule to move along a track using energy. In our specific case, we are using motility to refer to the ability of the dynein/dynactin/adapter complex to processively walk along a microtubule. We analyze three parameters to determine dynein's motility: the velocity at which the complex moves, the length the complex walks before falling off the microtubule (run length), and the number of motors walking when normalized to the length and number of microtubules. To test dynein/dynactin/spindly's motility, we took an *in-vitro* approach wherein we purified a GFP tagged spindly construct, mixed it with purified dynein and dynactin, and flowed it over fluorescently labeled microtubules. The dynein apparatus was allowed to bind to and walk along microtubules while a movie was acquired using Total Internal Reflection Fluorescence Microscopy (Figure 1A). The lengths of the GFP-spindly constructs purified were varied and spanned from 142 amino acids (GFP-spindly$^{1\text{-}142}$) to the full length 605 amino acid construct (GFP-spindly^{FL}) (Figure 1B). From these movies, we generated kymographs to determine the motility of the complex (Figure 1C). A kymograph is a graphical representation of the movement of a molecule over time. Time is plotted on the Y-axis, while the position of the molecule is plotted on the X-axis. Thus, the slope of the line on the kymograph correlates to the velocity of a single dynein complex. In this case, the more horizontal the line, the faster the complex moves.

Truncating Spindly and Determining Motility

The smallest fragment we initially tested was GFP-spindly$^{1-316}$, approximately half the size of the molecule. We found no discernable difference in motility of the dynein apparatus when using any of the constructs containing 316 or more amino acids (Figures 1C, 1E, 1F, 1G). From there, we truncated the protein further, down to GFP-spindly$^{1-142}$. GFP-spindly$^{1-142}$ and GFP-spindly$^{1-245}$ did not show any motility (data not shown). This was expected, as it has been shown previously that spindly requires its "spindly motif" to confer motility and neither of the above two constructs contain this motif (Gassmann et al. 2010). We also tested the motility of the dynein apparatus when using GFP-spindly$^{1-265}$ and GFP-spindly$^{1-275}$ as a cargo adapter and observed no change in motility as compared to GFP-spindly^{FL} (data not shown).

Forced Homodimerization of Spindly

We thought that perhaps dimerization of spindly could play a role in regulating SAC stripping, due to spindly's 2:2:2:2 stoichiometry with respect to the 3 components of the RZZ complex at the kinetochore, in addition to the fact that other dynein adapters form dimers when conferring motility (Mosalaganti et al. 2017; Urnavicious et al. 2015). We tested this by cloning a GST tag to the C-Terminus of spindly (Figure 2A). It has been shown that this GST tag induces homodimerization of the construct it is attached to (Reck-Peterson, 2006). The plan was to test two lengths of GST tagged adapters, GFP-spindly$^{1-316-GST}$ and GFP-spindly^{FL-GST}. However, we were unable to purify GFP-spindly^{FL-GST} due to poor expression and ineffective purification. GFP-spindly$^{1-316-GST}$ was purified however, and the motility of the dynein complex using GFP-spindly$^{1-316-GST}$ was compared to that of GFP-spindly$^{1-316}$. The dynein/dynactin/adapter complex showed a 1.6-fold increase in the number of motors walking when using GFP-spindly$^{1-316-GST}$ when compared to GFP-spindly$^{1-316}$ **(**Figure 2B-2E**)**. This increase is quite modest when compared to the change in motility of the dynein/dynactin/adapter complex when using truncated BicD2 compared to full length BicD2.

(Huynh et al, 2017). The velocity and run length remained unchanged. These experiments suggest that forcing a dynein effector into a homodimer could increase the motility of the dynein complex.

GFP-Spindly$^{1-275}$ Displays Characteristics Similar to Phase Separation

When attempting to purify GFP-Spindly$^{1-275}$, we made an interesting observation. Upon clarification of bacterial lysate at 4°C, a gelatinous substance formed at the bottom of the centrifuge tube. This gelatinous substance disappeared when warmed to room temperature and formed again when placed on ice. This behavior was reminiscent to proteins that undergo liquid-liquid phase separation, and so we investigated further whether this construct is phase separating. Phase separating proteins tend to form droplets on glass slides which can be imaged using either Differential Interface Contrast (DIC) or fluorescence microscopy (Lee et al. 2016; Woodruff et al. 2017). We were unable to visualize such droplets when imaging GFP-Spindly$^{1-275}$ suspended in 20mM HEPES pH 7.0 under both DIC and fluorescence microscopy (Figure 3A)**.** However, when 5mM $MgCl_2$ is added to the 20mM HEPES pH 7.0 (henceforth referred to as “droplet buffer”), droplets became visible under both DIC and fluorescence microscopy (Figure 3A).

We tested the motility of the dynein apparatus when using GFP-spindly$^{1-275}$ as a cargo adapter in conditions more conducive to phase separation (exact same conditions, except no EGTA is added). Interestingly, we again observed the formation of large GFP-spindly$^{1-275}$ droplets, which also contained dynein, and these droplets were motile along microtubules. This could indicate that when present in the droplets, GFP-spindly$^{1-275}$ is in a confirmation that promotes dynein/dynactin motility. However. When GFP-spindly$^{1-275}$ was incubated with dynein alone (no dynactin), we still observed motility (data not shown). Human dynein has been shown to be motile without dynactin present when tethered to a bead, presumably because the bead positions the dynein heads in a way analogous to dynactin (King et al. 2000; Nicholas et

al. 2015). Thus, it is also possible that the droplets of GFP-spindly$^{1-275}$ promote dynein motility in a similar manner.

In-vitro Characterization of Spindly Droplets

Droplets formed by phase separating proteins tend to dissipate when exposed to the alipathic alcohol 1,6 hexanediol (Kroschwald et al. 2015; Patel et al. 2007). We tested whether this applies to spindly droplets by adding 10% 1,6, hexanediol to droplet buffer during the droplet formation assay. Droplet formation drastically decreased as a result of 1,6 hexanediol addition (Figure 3A). To determine if these droplets form reversibly, we started with a tube of GFP-Spindly$^{1-275}$ in 20 mM HEPES 7.0. Fluorescence microscopy showed that no droplets formed (Figure 3C). Then $MgCl_2$ was added such that the final concentration of $MgCl_2$ was 5mM, and droplets were visualized under fluorescence microscopy. EDTA was then added to a final concentration of 5 mM to chelate the Mg_2. This resulted in a dramatically reduced number of droplets formed. When excess $MgCl_2$ was added to a final concentration of 10 mM $MgCl_2$, droplet formation was rescued to approximately 80% of what it was before EDTA was added. This suggests that the droplet formation is reversible and dependent on $MgCl_2$.

To further characterize these droplets, we suspended GFP-Spindly$^{1-275}$ in various buffers across a pH range from 4.0-8.0 (Figure 3E). We found droplets formed optimally at a pH of 7.0. While suspending GFP-spindly$^{1-275}$ in droplet buffer pH 7.0 yielded the most droplets in this experiment, suspending GFP-spindly$^{1-275}$ in droplet buffer pH 8.0 yielded very few droplets, showing a strong sensitivity to pH. To test the sensitivity to monomeric salt, different concentrations (from 0-50 mM) of NaCl was added to droplet buffer and the ability to form droplets was tested (Figure 3G). Another truncated dynein cargo adapter, GFP-BicD$^{25-400}$ was also purified with the same tags as GFP-spindly$^{1-275}$. GFP-BicD$^{25-400}$ did form some droplets, though they were fewer in number compared to GFP-spindly$^{1-275}$. As the concentration of NaCl

increased, the number of droplets formed decreased for both proteins, though the GFP-spindly droplets were more robust in number than the GFP-BicD2$^{25-400}$ droplets.

Additionally, we tested GFP-Spindly constructs of varying lengths to determine which domains of spindly are sufficient for droplet formation (Figure 3I). The smallest construct, GFP-Spindly$^{1-142}$ did not form droplets, while the next longest construct, GFP-Spindly$^{1-245}$ did. While GFP-Spindly$^{1-265}$ and GFP-Spindly$^{1-275}$ formed droplets, GFP-Spindly$^{1-316}$ did not. Finally, GFP-Spindly^{FL} formed a few droplets, indicating the full-length construct has the capacity to form droplets under the right conditions.

Computational Analysis of Local Amino Acid Composition of Spindly

To learn more about the formation of these droplets, we turned to a computational approach developed in the lab of Dr. Eric Ross. Dr. Sean Cascarina ran the primary sequence of spindly through an algorithm that uses a sliding window to determine the local concentration of amino acids (Figure 4). What stuck out the most was the concentration of glutamic acids near the N-terminus of the protein. While most phase separating proteins tend to have polar or hydrophobic amino acids clustered together, it is not unprecedented for proteins undergoing phase separation to have high glutamic acid content. For example, phase separation of the yeast prion protein Sup35 seems to be dependent on a highly charged domain (Franzmann et al. 2018). Due to both the high glutamic acid abundance in GFP-Spindly$^{1-275}$, and the dependence of magnesium for droplet formation, it is possible the magnesium is coordinating the negative charge of multiple glutamic acids in order to facilitate droplet formation. This would also explain why sodium can interrupt droplet formation, as it cannot coordinate the negative charge of the glutamic acids, instead acting as a counter ion.

GFP-spindly$^{1-275}$ Forms Dynamic, Fusible Droplets in Vivo

To determine whether these droplets are formed within the context of a cell, Amy Hodges and Suzy Hoser, a masters student and undergraduate in the lab, respectively, cloned GFP- Spindly$^{1-275}$ under control of a CMV promotor and transiently transfected HeLa cells with the plasmid, and determined if droplets formed within the cells via confocal fluorescence microscopy (Figure 5A). Of the cells that had been properly transfected (as determined by thresholding the total fluorescence in the cell) 30% formed droplets, compared to .66% of cells forming droplets when transfected with the full length GFP-Spindly construct (Figure 5B). Interestingly, these droplets were dynamically moving around in the cell, and would fuse with another droplet in some instances (Figure 5C). This again lends credence to the hypothesis that GFP-Spindly$^{1-275}$ undergoes phase separation, as other phase separating proteins display similar properties. As the full length construct seems to display the potential for droplet formation (figure 3I), it will be interesting in the future to determine whether this behavior is an artifact of truncating the protein, or if there is regulation in the cell that can tune spindly's ability to undergo phase separation, perhaps relating to the expansion of the fibrous corona.

Discussion

The inability of spindly truncations smaller than 246 amino acids to confer motility to the dynein complex isn't surprising, as those truncations do not contain the spindly motif previously discovered to be required for dynein motility. However, how well the larger truncations facilitate the motility of the dynein complex had yet to be investigated prior to this study. In contrast to BicD2, truncating the C-terminal half of the coiled coil that isn't essential for dynein motility did not result in an increase in the number of motors moving along microtubules. There may yet still be other means of regulating the dynein/dynactin/spindly complex's motility however, as spindly is known to be subject to various post-translational modifications, such as phosphorylation by the mitotic kinase MPS-1, and farnesylation, and these modifications were not tested in this study.

Alternatively, perhaps kinetochore localized dynein is already as active as it needs to be at the kinetochore, and the only requirement of SAC stripping is a microtubule for dynein to walk on. Dynein/dynactin/spindly has previously been observed as a complex with poor motility compared to a dynein complex using other cargo adapters, so it is attractive to think that the motility may be improved (McKenney et al. 2014). However, kinetochore-localized dynein is involved in other mitotic functions, such as spindle assembly, dictating the orientation of the mitotic spindle, and the conversion of lateral to end on kinetochore microtubule attachments (Merdes et al 1996; O'Connell et al. 2000; Varma et al. 2008). Perhaps the low motility of the dynein/dynactin/spindly complex is a feature to make sure that SAC stripping doesn't result in too much loss of kinetochore localized dynein such that it cannot perform its other functions.

While truncation of spindly did not yield any effect on the motility of the dynein/dynactin/spindly complex, it did seem to affect the properties of spindly itself. Namely,

truncated spindly constructs consisting of approximately the N-terminal 250 amino acids showed a propensity to phase separate. To date, kinetochore proteins in a physiological context have not been implicated with phase separation, so this behavior could potentially represent a new way of thinking about the interactions of proteins at the kinetochore, particularly the fibrous corona. In addition, GFP-spindly^{FL} did form droplets in certain conditions (Figure 3I) though to a lesser degree than GFP-Spindly$^{1-275}$. This indicates the full construct has the capacity to phase separate, and that truncating the C-terminal half increases the protein's propensity to do so.

Additionally, phase separation appears to be dependent on Mg^{2+}. This could be a result of the many glutamic acids clustered in the N-terminal half of spindly. Because Mg^{2+} has the capacity to coordinate several negative charges, perhaps Mg^{2+} is coordinating glutamic acids from various spindly molecules to form a sort of "seed" which expands out from there (Figure 6). This would further explain the sensitivity to sodium, as sodium would act as more of a counter-ion to the negative glutamic acids, rather than an ion that would coordinate multiple negative charges.

Spindly and the RZZ complex have long been implicated in forming the fibrous corona, and recently, have been implicated in driving corona expansion during a stalled prometaphase. Recent papers discuss spindly auto-inhibition as a possible mechanism for regulating this expansion (Pereira et al. 2018; Rodriguez-Rodriguez et al. 2018; Sacristan et al. 2018). The authors show spindly forming long filaments in cells when tethered to the kinase MPS-1, and propose that the RZZ complex plus spindly forms these filaments on the kinetochore during corona expansion. Spindly's auto-inhibition is reminiscent of another dynein effector, BicD2, which folds back on itself in an auto-inhibitory fashion. This auto-inhibition is removed upon binding to cargo (McClintock et al, 2018; Pereira et al. 2018; Rodriguez-Rodriguez et al. 2018; Sacristan et al. 2018). Spindly's auto-inhibition is presumably removed through some

combination of farnesylation of spindly's most c-terminal cysteine, and phosphorylation by MPS-1.

In this study, we propose the possibility that the mechanism of spindly driving corona expansion is through phase separation, rather than filament formation. *In-vitro* characterization of spindly truncations is consistent with many phase separating proteins, including a sensitivity to pH, monomeric salt, and 1,6 hexane-diol. When transfected into cultured human cells, the truncation formed dynamic, fusible aggregates in the cell, indicating phase separation can occur under physiological conditions.

It is unclear in this study if magnesium is specifically required to facilitate phase separation, or if any divalent cation will suffice. A recent report suggested levels of free magnesium rise during mitosis, so it would be interesting to see if corona expansion is dependent on this increase in magnesium (Maeshima et al 2018).

While this study establishes the possibility of phase separation of spindly at the kinetochore, it doesn't directly demonstrate spindly phase separating at the kinetochore. One experiment that would be interesting to run would be to arrest HeLa cells expressing GFP-spindly in metaphase with the microtubule depolymerizing drug nodocozole. Once it is confirmed that fibrous corona expansion is occurring, 1,6 hexanediol could be added to disrupt phase separating behavior within the cell. If the fibrous corona dissolves as a result of 1,6 hexanediol addition, that would lend credence to the hypothesis that spindly phase separation is driving corona expansion.

Additionally, the N values of some of the experiments in this study are rather low, particularly in figure 3. While the trends shown in figure 3 seem rather drastic, additional technical replicates are required to further verify the results.

Finally, it would be interesting to try to determine conditions in which the purified full-length spindly construct can phase separate *in vitro* similarly to GFP-spindly$^{1-275}$, perhaps due to phosphorylation by MPS-1, farnesylation of the most C-terminal Cystine, or some other mechanism.

Materials and Methods

Plasmid Generation

To generate the plasmid containing GFP-spindly^{FL}, spindly cDNA (gift from Rick Mckenney) was amplified by PCR and ligated into the PET28A vector (gift from Rick McKenney). To generate GFP-spindly truncation constructs, the appropriately sized fragment was amplified using PCR from the full length Pet28A spindly construct. The full length vector was then digested with KpnI and NotI**.** The PCR fragment was then ligated into the digested vector using Gibson assembly, according to the manufacturer's instructions**.** The resulting spindly truncation was thus N-Terminally tagged with 6HIS, strep, and GFP, in that order. Successful PCR and ligation was then confirmed by sequencing.

Purification of Dynein Adapters

Plasmids containing GFP-spindly constructs were transformed into BL-21 RIPL cells (Aligent) and plated on LB agar with the appropriate antibiotic. Cells were then grown in LB media (affymetrix) at 37° C at 200 rpm to an OD600 of .500-.800. IPTG was added to a final concentration of 1mM, and the temperature was shifted to 16°C. The cells were grown in these conditions overnight and were harvested by centrifugation at 6000G at 4°C for 15 minutes. Cell pellets were harvested and either stored at -80°C or immediately lysed and the protein was purified.

To purify the non-phase separating spindly constructs, along with BicD^{N}, cell pellets were mixed with lysis buffer (30mM HEPES, 50mM Potassium Acetate, 2mM Magnesium Acetate, 10% Glycerol, 1mM EDTA. Buffer was then pHed to 7.4) at a ratio of 9mL of lysis buffer per 1L of culture and lysed via microfluidization. Lysate was clarified via ultra-centrifugation at 90,000G for 30 minutes at 4° C. The lysate was then put over pre-equilibrated

strep-tactin superflow plus beads (Qiagen) for 1-3 hours. GST-spindly$^{1\text{-}316_GST}$ was purified using Pierce® Glutathione Agarose beads (ThermoFisher Scientific). The beads were washed three times with 5mL of lysis buffer, and then added to a disposable 2mL Polystyrene column (ThermoFisher Scientific). 5mL of elution buffer (30mM HEPES, 50mM Potassium Acetate, 2mM Magnesium Acetate, 10% Glycerol, 1mM EDTA, and either 5mM d-Desthiobiotin for strep-tactin beads, or 1mM reduced-Glutathione for Glutathione beads**)** was added to elute the protein off the strep-tactin beads. Eluates were then concentrated (Amicon) and run over a Superose 6 Increase 10/300 GL gel filtration column (GE Life Sciences) using Gel Filtration Buffer (30mM HEPES, 50mM Potassium Acetate, 2mM Magnesium Acetate, 10% Glycerol, 100mM NaCl). Eluates off the filtration column were then either further concentrated and flash frozen with liquid N2, or just flash frozen with liquid N2. Proteins were then stored at -80°C.

Purification of the phase separating spindly constructs was performed similarly as above, with one modification. Cell pellets were mixed with lysis buffer as above and lysed by microfluidization. The lysate was then centrifuged at 90,000G for 30 minutes at 4°C. Pre-equilibrated Strep-Tactin Superflow Plus beads were added to the lysate and incubated on a rotator at 4°C for 1-3 hours. After three washes with 5mL lysis buffer, the protein was eluted off the beads in batch, using elution buffer. Due to uncertainty with how the phase separating protein would behave on a column, the protein was not gel filtered. The protein was then flash frozen in liquid nitrogen and stored at -80°C.

Droplet Formation Assay

The indicated Spindly truncation was gently mixed with the indicated buffer at a final concentration of 640 nM, and 7ul of the solution was spotted to a glass slide (ThermoFisher Scientific). Both DIC and fluorescence images were taken (see image acquisition) and analyzed in imageJ. The number of droplets visible under DIC microscopy was counted, and in ambiguous cases, the 488 channel was merged with the DIC channel to determine the extent

of overlap between the two channels. If a green droplet co-localized with a punitive droplet under DIC, it was counted as a droplet. If there was no co-localization, it was not counted.

Single Molecule Motility Assay

The single molecule motility assay was performed on homemade flow chambers. A flow chamber is made of a glass slide adhered to a plasma cleaned and salinized coverslip (ThermoFisher Scientific) via double sided tape, leaving a chasm between two pieces of tape approximately 7-10 ul in volume. Anti-Tubulin antibodies (8 µg/ml, YL1/2; Accurate Chemical & Scientific Corporation) are then flowed into the chamber and incubated for five minutes. 1% Pluronic F-127 (ThermoFisher Scientific) is then added to the flow chamber as a blocking agent as the solution containing antibodies that didn't bind to the coverslip are simultaneously absorbed from the flow chamber using a KimWipe. Pluronic F-127 is incubated on the coverslip for two minutes. TIRF Assay Buffer (50mM HEPES, 10mM Magnesium Sulfate, 2mM EGTA, 2mM DTT, 20uM taxol) is then flowed into the chamber to wash unnecessary blocking agent off. Fluorescently labeled, taxol stabilized microtubules are then added to the flow chamber and allowed to incubate until they have bound to the antibodies, usually 2-5 minutes, but the microtubules are monitored on the microscope to ensure proper saturation. The microtubules are assembled from unlabeled and HiLyte647-labeled porcine tubulin in a 10:1 ratio respectively (Cytoskeleton). TIRF Assay Buffer is then flowed over the microtubules to wash off excess microtubules.

While this is happening, dynein and dynactin (gift from Rick McKenney) were incubated with 400 nM of the dynein cargo adapter for 15 minutes. Afterword, 3 ul of the dynein/dynactin/adapter solution was mixed with 7 ul of activation buffer (50mM HEPES, 10mM Magnesium Sulfate, 2mM EGTA, 2mM DTT, 20uM taxol, 1mM ATP, 143mM 2-mercaptoethanol), and flowed into the coverslip as images were acquired at 1s intervals for 5 minutes. Velocity, run length, and the number of motile motors were determined from

kymographs generated from the MultipleKymograph plugin in ImageJ, as previously described **(**Reck-Peterson et al. 2006).

Computational Analysis for the Primary Sequence of Spindly^{FL}

The Computational analysis done in figure 4 was performed as previously described (Cascarina et al. 2018). Briefly, the algorithm took a sliding window and calculated the percent composition for each amino acid in that window. The values in figure 4 correlate to the maximum percent composition observed for the indicated amino acid and window size (from 10 to 100).

Image Acquisition

All images taken for single molecule motility assays were taken on a 1.49 NA 100x TIRF objective on a Nikon Ti-E inverted microscope with a Ti-S-E motorized stage piezo Z-control (Physik Instrumente), with an iXon x 3 DU897 cooled EM-CCD camera (Andor). 488nm and 640nm lasers (Coherent) were used with a multi pass quad filter cube set (C-TIRF for 405/488/561/640 nm; Chroma) and emission filters mounted in a filter wheel (525/50nm, 600/50 nm, 700/75nm; Chroma) were used to image GFP-adapter truncations and HiLyte647-microtubules respectively.

All images taken for the live cell droplet formation assay were acquired on an IX71 inverted microscope (Olympus) incorporated into a DeltaVision Personal DV imaging system (GE Healthcare) with a 40× 0.75 NA UPlanFl lens (Olympus) and a CoolSNAP HQ2 camera. softWoRx acquisition software (Applied Precision) was used to control the system. Images were analyzed in DeltaVision Personal DV imaging system (GE Healthcare) using SoftWoRx software (GE Healthcare). Images taken has their the background fluorescence intensity calculated, and cells with high enough expression were checked to see if the spindly truncation formed droplets within the cell.

Images taken for the *in-vitro* droplet characterization experiment were on a spinning disc confocal scanner (CSUX1; Yokogawa) using a GFP emission filter (ET525/50 M), with both a DIC source and a 488 nm laser (housed in an LU-NV unit with AOTF control; Nikon). The microscope was controlled with NIS Elements software (Nikon).

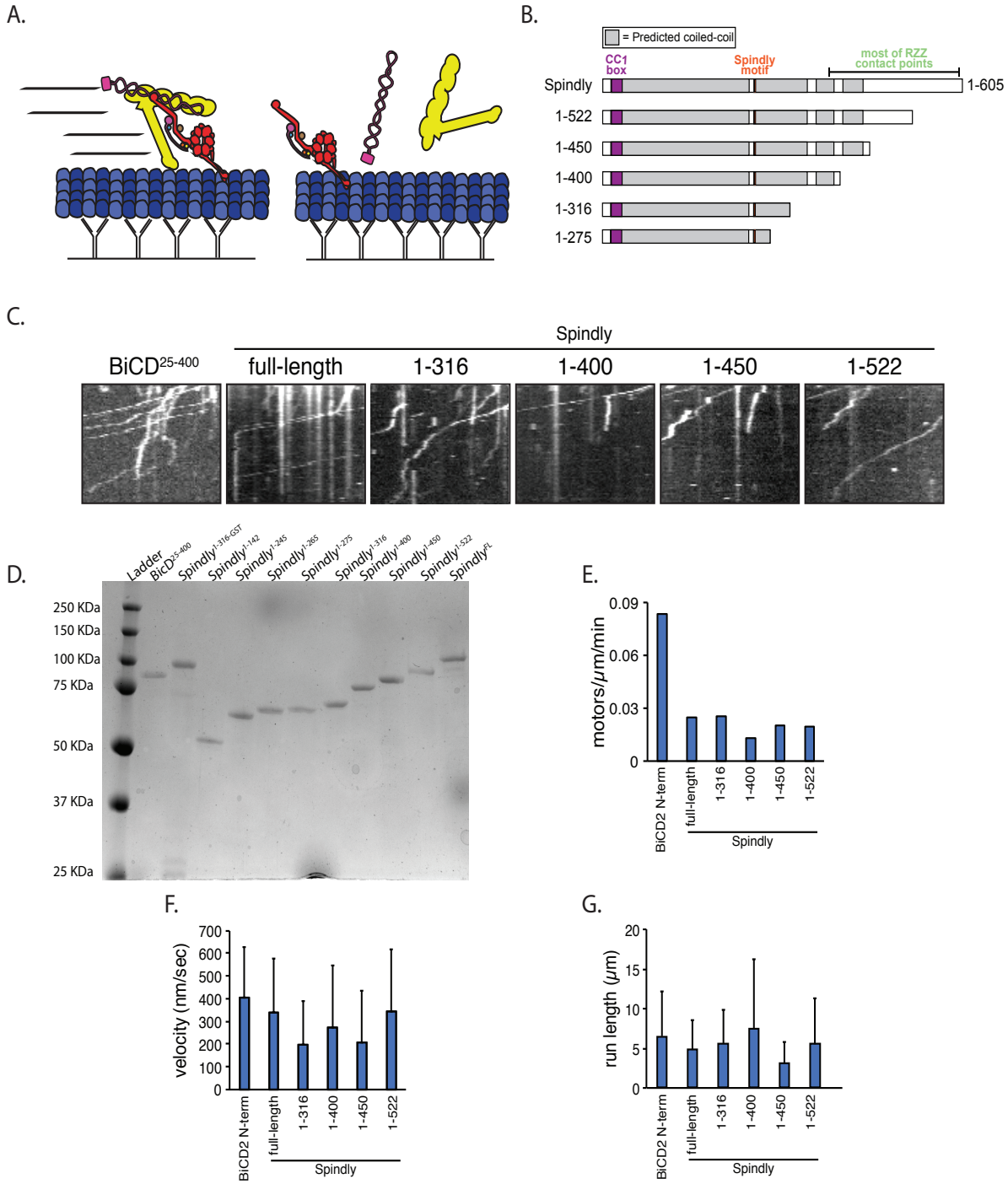

Figure 1. Truncating spindly to approximately half its length has no discernable effect on the motility of the dynein/dynactin/spindly complex *in-vitro*.

(Figure legend continued on next page)

Figure 1. (continued)

(A.) Schematic of experimental design of single molecule motility assay. Briefly, fluorescently labeled microtubules are attached to salinized coverslips via anti tubulin antibodies. Dynein/dynactin and the indicated adapter are incubated together for 15 minutes before they are introduced to microtubules and motility is allowed. A movie is acquired while dynein is walking along the microtubules which allows for the quantification of parameters relating to the motility of the complex.

(B.) Schematic of all spindly truncations used in this figure.

(C.) Kymographs of single molecule motility assay performed using indicated truncation.

(D.) Coomassie stained 7.5% SDS-PAGE of GFP-spindly truncations used in this study.

(E.) – (G.) Graphs depicting motility of the dynein complex using indicated adapter. **(E.)** depicts the number of motors walking along microtubules when normalized to the amount and length of microtubules. **(F.)** shows the velocity of the complex, while **(G.)** depicts how long the motors walked before falling off the microtubule.

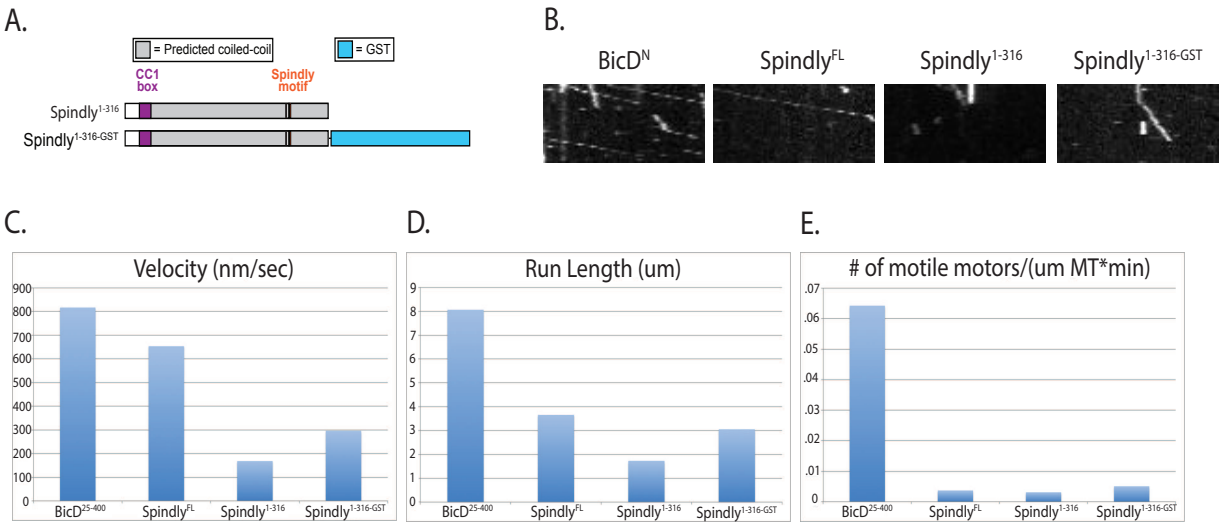

Figure 2. Motility of the dynein/dynactin/spindly complex is slightly improved upon forced homodimerization.

A.) Schematic of the GFP-spindly constructs of interest.

B.) Kymographs of dynein/dynactin/indicated adapter. Experiments were run as described in Figure 1B.

C.) – E.) Quantification of the movies taken in **B**. **C.)** depicts the velocity of the motor in nm/sec. **D.)** depicts how long the motor walked along the microtubule before falling off (run length). **E.)** depicts the number of motile motors, normalized to the length of microtubules and video length.

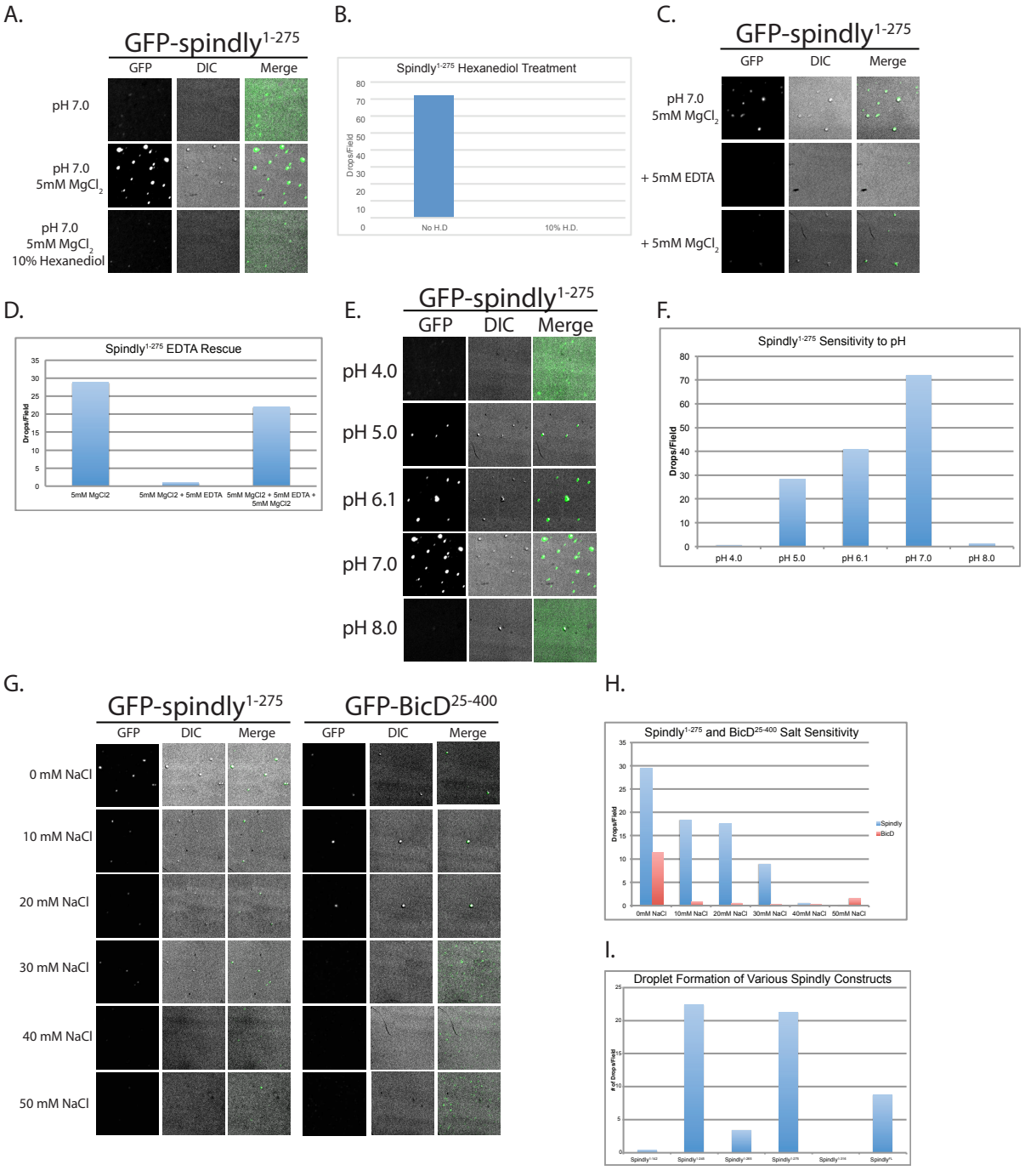

Figure 3. *In-vitro* characterization of GFP-spindly$^{1-275}$ droplets.

(Figure legend continued on next page)

Figure 3. (Continued)

(A.) Representative cropped fields of GFP-spindly$^{1-275}$ droplets forming on a glass coverslip. GFP-spindly$^{1-275}$ was gently mixed with 20mM HEPES at pH 7.0 (top row), 20mM HEPES, 5mM $MgCl_2$ at pH 7.0 (middle row) or 20mM HEPES, 5mM $MgCl_2$, 10% 1,6 Hexanediol at pH 7.0 (bottom row) at a final concentration of 640nM and 7ul were immediately spotted on a glass cover slip and imaged.

(B.) Quantification of **A.** Only drops found under DIC microscopy were counted in the quantification. The addition of 10% 1,6 Hexanediol completely abolished droplet formation.

(C.) Representative cropped fields of GFP-Spindly$^{1-275}$ showing sensitivity to EDTA, and rescue by adding excess $MgCl_2$. GFP-spindly$^{1-275}$ was first gently mixed in droplet buffer and imaged as in A (top row). EDTA was then added and gently mixed to a final concentration of 5mM and 7ul were added to a glass coverslip and imaged (middle row). Finally, $MgCl_2$ was added such that the final concentration of $MgCl_2$ was 10mM, gently mixed, and imaged in the same way as the rest of the experiment (bottom row).

(D.) Quantification of **C.** The addition of EDTA abolished droplet formation, yet adding excess $MgCl_2$ rescued droplet formation to approximately 80%.

(E.) Representative cropped fields of GFP-spindly$^{1-275}$ showing sensitivity to changes in pH. Because there is no buffer that effectively works at all indicated pH's, several different buffers were used. 200mM Sodium Acetate was used for pH's 4.0 and 5.0 (top two rows) (concentration) of PIPES was used for the pH of 6.1 (middle row), and 20mM HEPES was used for Ph's 7.0 and 8.0 (bottom two rows). All buffers contained 5mM $MgCl_2$.

(F.) Quantification of **E.** Generally, GFP-spindly$^{1-275}$ formed droplets more readily as the pH of the buffer approached 7.0, with a sharp drop off from pH 7.0 to pH 8.0. This drop off cannot be explained by the use of different buffers, as 20mM HEPES was used at both pH's.

(G.) Representative cropped fields of GFP-spindly$^{1-275}$ and GFP-BicD^{N} showing sensitivity to NaCl. Either GFP-spindly$^{1-275}$ or GFP-BicD^{N} was added and gently mixed with droplet buffer that also contains the indicated concentration of NaCl. Images were obtained similarly to previous panels.

(H.) Quantification of **G.** GFP-spindly$^{1-275}$ formed more droplets than GFP-BicD^{N} and spindly$^{1-275}$ droplets were less sensitive to NaCl than their BicD^{N} counterparts.

(I.) Indicated GFP-spindly truncation was added to droplet buffer and images were obtained the same as in other panels. The quantification of this experiment is shown here. GFP-spindly$^{1-142}$ and GFP-spindly$^{1-316}$ did not form droplets. GFP-spindly$^{1-245}$ and GFP-spindly$^{1-275}$ formed the most droplets, while GFP-spindly$^{1-265}$ and GFP-spindly^{FL} formed few droplets.

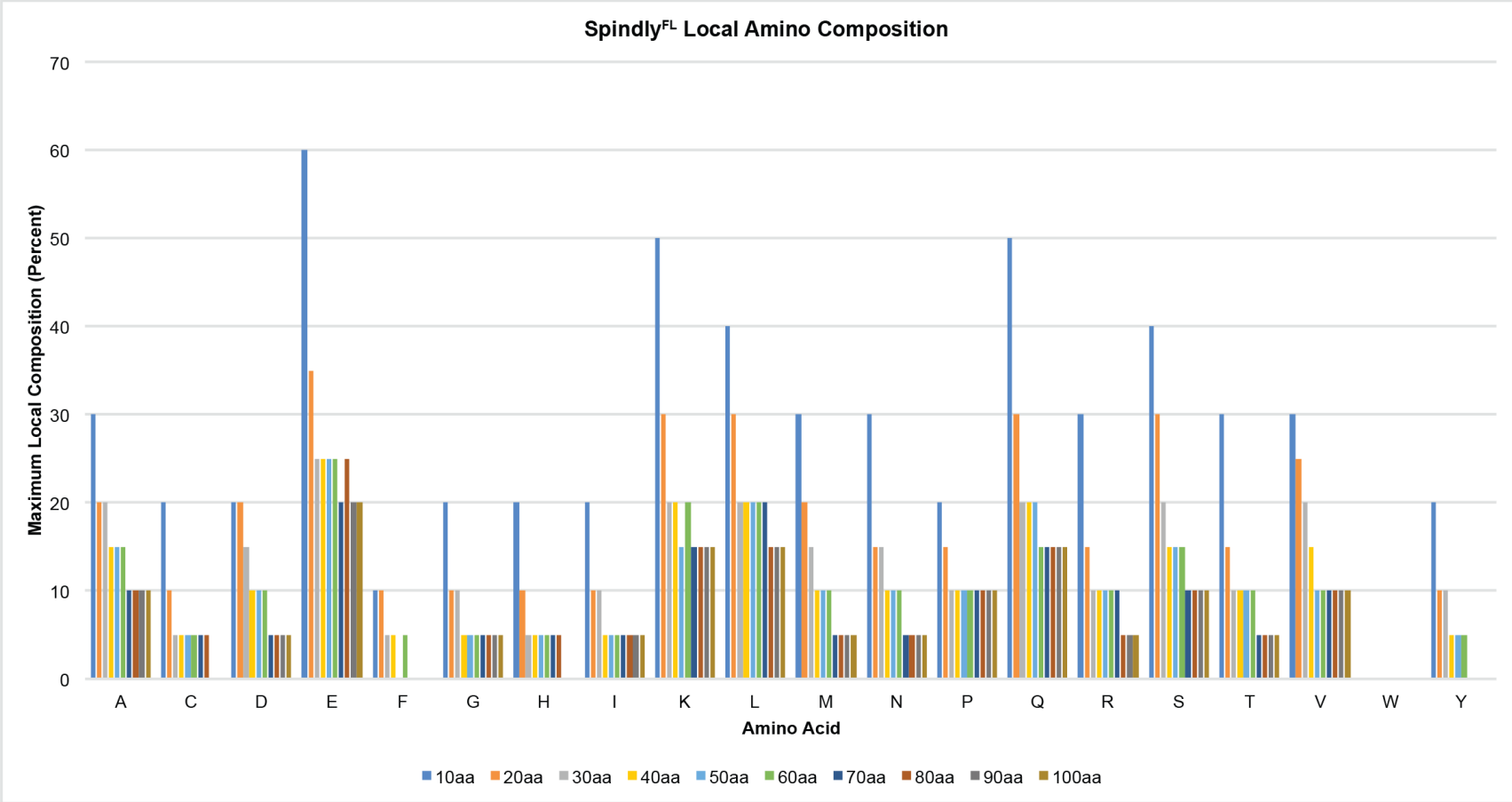

Figure 4. Dr. Sean Cascarina's computational analysis of spindly's local amino acid composition. Briefly, Dr. Cascarina's script takes a sliding window of various sizes (indicated by color) and determines the most predominant amino acid in that window. Higher bars for a particular amino acid correlate to greater local abundance.

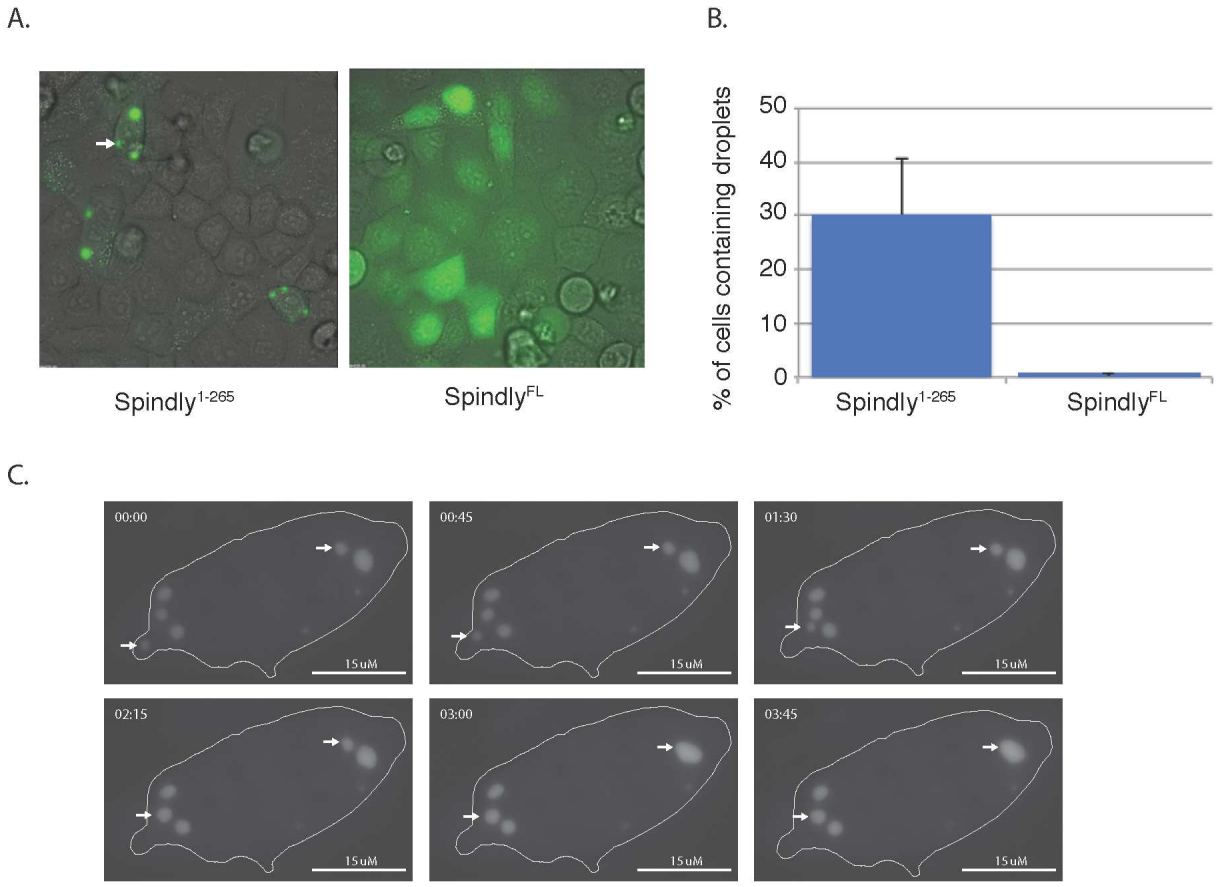

Figure 5. Live cell transfection of GFP-spindly$^{1-265}$.

A.) GFP-spindly$^{1-265}$ (left) and GFP-spindly^{FL} (right) were transiently transfected into separate flasks containing Kyoto HeLa cells, and imaged via fluorescence microscopy. The number of cells containing dynamic fluorescent droplets were compared between the two transfections. Arrow indicates one such droplet.

B.) Quantification of **A.** GFP-spindly$^{1-265}$ contained significantly more droplets than GFP-spindly^{FL}.

C.) Time lapse of a Kyoto HeLa cell that has been transiently transfected with GFP-spindly$^{1-265}$. Arrows indicate droplets that move in the cell and fuse into other droplets.

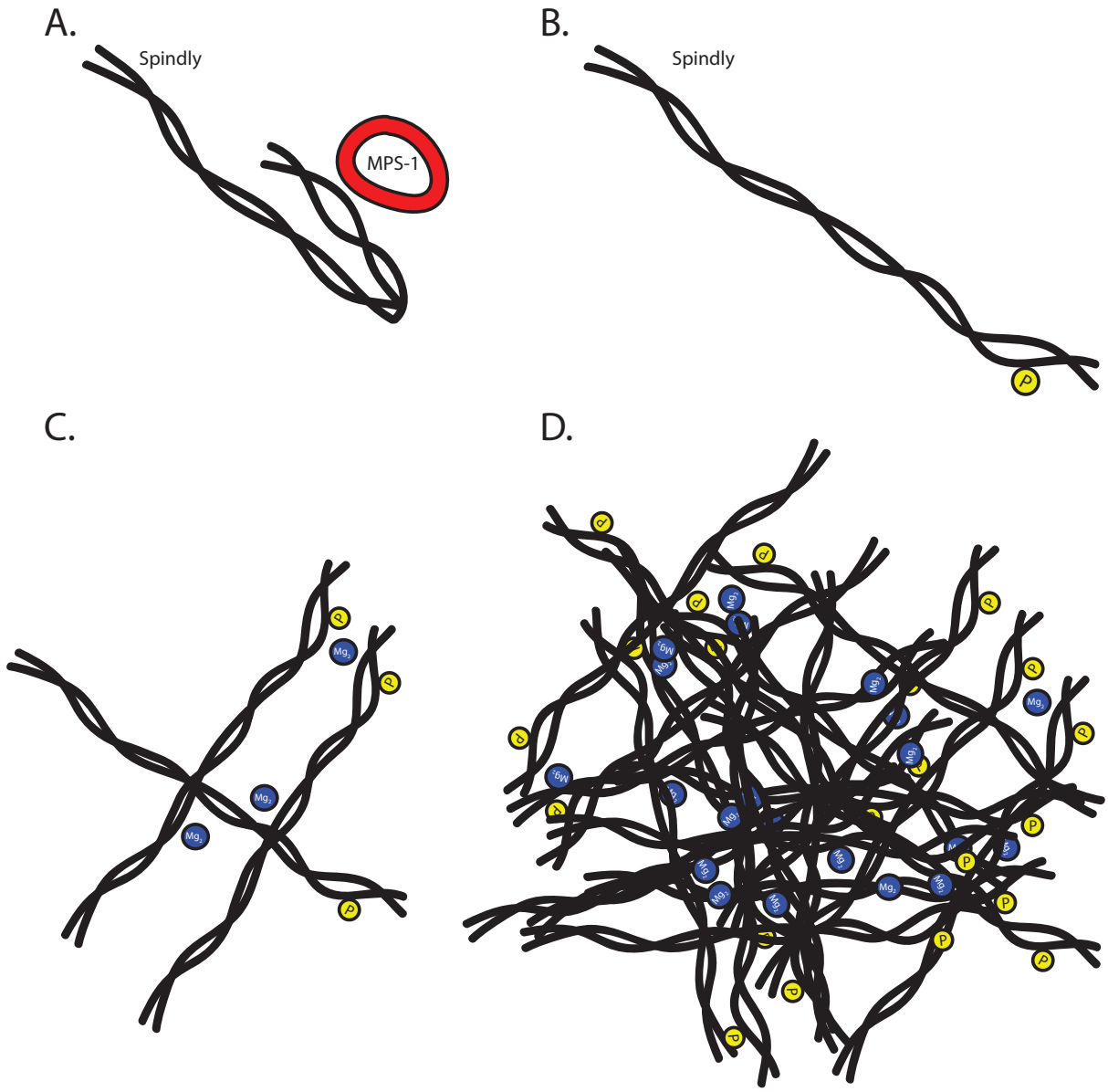

Figure 6. Proposed model for spindly phase separation.

A.) Spindly first becomes phosphylorated by the mitotic kinase MPS-1.

B.) As a result of phosphyloration, and other potential mechanisms, spindly auto-inhibition is released.

C.) Spindly can now interact with other spindly molecules, aided by the presence of magnesium.

D.) These transient, dynamic interactions fuel corona expansion by recruiting more spindly to an unattached kinetochore.

References

Barisic, M., Sohm, B., Mikolcevic, P., Wandke, C., Rauch, V., Ringer, T., . . . Geley, S. (2010). Spindly/CCDC99 Is Required for Efficient Chromosome Congression and Mitotic Checkpoint Regulation. *MBOC, 21*(12), 1968-81.

Caldas, G., Lynch, T., Anderson, R., Afreen, S., Varma, D., & DeLuca, J. (2015). The RZZ complex requires the N-terminus of KNL1 to mediate optimal Mad1 kinetochore localization in human cells. *Open Biology, 5*(11).

Cascarina, S., & Ross, E. (2018, 9 24). Proteome-scale relationships between local amino acid composition and protein fates and functions. *PLoS computational biology, 14*(9), e1006256-e1006256.

Chan, Y., Fava, L., Uldschmid, A., Schmitz Michael, Gerlich, D., Nigg, E., & Santamaria, A. (2009). Mitotic control of kinetochore-associated dynein and spindle orientation by human Spindly. *Journal of Cell Biology, 185*(5), 859-874.

Cheeseman, I., & Desai, A. (2008, 1 1). Molecular architecture of the kinetochore–microtubule interface. *Nature Reviews Molecular Cell Biology, 9*, 33.

Cimini, D., Moree, B., Canman, J., & Salmon, E. (2003). Merotelic kinetochore orientation occurs frequently during early mitosis in mammalian tissue cells and error correction is achieved by two different mechanisms. *Journal of Cell Science, 116*, 4213-4225.

Daum, J., Potapove, T., Sivakumar, S., Daniel, J., Flynn, J., Rankin, S., & Gorbsky, G. (2011). Cohesion Fatigue Induces Chromatid Separation in Cells Delayed at Metaphase. *Current Biology, 21*(12), 1018-1024.

DeLuca, J., & Musacchio, A. (2012, 2). Structural organization of the kinetochore-microtubule interface. *Current opinion in cell biology, 24*(1), 48-56.

Desai, A., Rybina, S., Müller-Reichert, T., & Shevchenko, A. (2003). KNL-1 directs assembly of the microtubule-binding interface of the kinetochore in C. elegans. *Genes and Development, 17*(19), 2421-2435.

Fang, G., Yu, H., & Kirschner, M. (1998). The checkpoint protein MAD2 and the mitotic regulator CDC20 form a ternary complex with the anaphase-promoting complex to control anaphase initiation. *Genes and Development, 12*(12), 1871-1873.

Franzmann, T., Jahnel, M., Pozniakovsky, A., Mahamid, J., Holehouse, A., Nüske, E., . . . Alberti, S. (2018, 1 5). Phase separation of a yeast prion protein promotes cellular fitness. *Science, 359*(6371), eaao5654.

Gama, J., Pereira, C., Simões, P., Celestino, R., Reis, R., Barbosa, D., . . . Gassmann, R. (2017). Molecular mechanism of dynein recruitment to kinetochores by the Rod-Zw10-Zwilch complex and Spindly. *J Cell Biol, 216*(4), 943-960.

Gassmann, R., Holland, A., \arma, D., Wan, X., Civril, F., Cleveland, D., . . . Desai, A. (2010). Removal of Spindly from microtubule-attached kinetochores controls spindle checkpoint silencing in human cells. *Genes Dev, 9*, 957-971.

Griffis, E., Stuurman, N., & Vale, R. (2007). Spindly, a novel protein essential for silencing the spindle assembly checkpoint, recruits dynein to the kinetochore. *The Journal of Cell Biology, 177*(6), 1005-1015.

Heasley, L., Markus, S., & DeLuca, J. (2017, 3 15). "Wait anaphase" signals are not confined to the mitotic spindle. *Molecular Biology of the Cell, 28*(9), 1186-1194.

Holland, A., Reis, R., Niessen, S., Pereira, C., Andres, D., Spielmann, P., . . . Gassman, R. (2015). Preventing farnesylation of the dynein adaptor Spindly contributes to the mitotic defects caused by farnesyltransferase inhibitors. *Molecular Biology of the Cell, 26*(10), 1845-56.

Hoogenraad, C., Wulf, P., Schiefermeier, N., Stepanova, T., Galjart, N., Small, J., . . . Akhmanova, A. (2003). Bicaudal D induces selective dynein-mediated microtubule minus end-directed transport. *EMBO*, 1-12.

Howell BJ, McEwen BF, Canman JC, Hoffman DB, Farrar EM, Rieder CL, S. (2001). Cytoplasmic dynein/dynactin drives kinetochore protein transport to the spindle poles and has a role in mitotic spindle checkpoint inactivation. *J Cell Biol, 155*(7), 1159-72.

Huynh, W., & Vale, R. (2017, 10 2). Disease-associated mutations in human BICD2 hyperactivate motility of dynein–dynactin. *The Journal of Cell Biology, 216*(10), 3051.

Kelley, L., Mezulis, S., Yates, C., Wass, M., & Sternberg, M. (2015). The Phyre2 web portal for protein modelling, prediction and analysis. *Nature Protocols, 10*(6), 845-858.

King, R., Peters, J.-M., Tugendreich, S., Rolfe, M., Hieter, P., & Kirschner, M. (1995). A 20s complex containing CDC27 and CDC16 catalyzes the mitosis-specific conjugation of ubiquitin to cyclin B. *Cell, 81*(2), 288.

King, S., & Schroer, T. (2000). Dynactin increases the processivity of the cytoplasmic dynein motor. *Nature Cell Biology, 2*(1), 20-24.

Kroschwald, S., Maharana, S., Mateju, D., Malinovska, L., Nüske, E., Poser, I., . . . Alberti, S. (2015). Promiscuous interactions and protein disaggregases determine the material state of stress-inducible RNP granules. (J. Kelly, Ed.) *eLife, 4*, e06807.

Lee, K.-H., Zhang, P., Kim, H., Mitrea, D., Sarkar, M., Freibaum, B., . . . Taylor, J. (2016). C9orf72 Dipeptide Repeats Impair the Assembly, Dynamics, and Function of Membrane-Less Organelles. *Cell, 167*(3), 774-788.e17.

Li, X., & Nicklas, B. (1995). Mitotic forces control a cell-cycle checkpoint. *Nature, 373*, 630-632.

Li, Y., Gorbea, C., Mahaffey, D., Rechsteiner, M., & Benezra, R. (1997). MAD2 associates with the cyclosome/anaphase-promoting complex and inhibits its activity. *PNAS, 94*(23), 12431-12436.

Maciejowski, J., Drechsler, H., Grundner-Culemann, K., Ballister, E., Rodriguez-Rodriguez, J.-A., Rodriguez-Bravo, V., . . . Jallepalli, P. (2017). Mps1 Regulates Kinetochore-Microtubule

Attachment Stability via the Ska Complex to Ensure Error-Free Chromosome Segregation. *Developmental Cell, 41*(2), 143-156.

Maeshima, K., Matsuda, T., Shindo, Y., Imamura, H., Tamura, S., Imai, R., . . . Nagai, T. (2018, 2 5). A Transient Rise in Free Mg2+ Ions Released from ATP-Mg Hydrolysis Contributes to Mitotic Chromosome Condensation. *Current Biology, 28*(3), 444-451.e6.

Magidson, V., O'Connell, C., Lončarek, J., Paul, R., Mogilner, A., & Khodjakov, A. (2011). The Spatial Arrangement of Chromosomes during Prometaphase Facilitates Spindle Assembly. *Cell, 146*(4), 555-567.

Magidson, V., Paul, R., Yang, N., Ault, J., O'Connell, C., Tikhonenko, I., . . . Khodjakov, A. (2015). Adaptive changes in the kinetochore architecture facilitate proper spindle assembly. *Nat Cell Biol, 17*(9), 1134-1144.

McClintock, M., Dix, C., Johnson, C., McLaughlin, S., Maizels, R., Hoang, H., & Bullock, S. (2018). RNA-directed activation of cytoplasmic dynein-1 in reconstituted transport RNPs. (A. Musacchio, Ed.) *eLife, 7*, e36312.

McKenney, R., Huynh, W., Tanenbaum, M., Bhabha, G., & Vale, R. (2014). Activation of cytoplasmic dynein motility by dynactin-cargo adapter complexes. *Science, 345*(6194), 337-341.

Merdes, A., Ramyar, K., Vechio, J., & Cleveland, D. (1996, 11 1). A Complex of NuMA and Cytoplasmic Dynein Is Essential for Mitotic Spindle Assembly. *Cell, 87*(3), 447-458.

Mosalaganti, S., Keller, J., Altenfeld, A., Winzker, M., Rombaut, P., Saur, M., . . . Musacchio, A. (2017). Structure of the RZZ complex and molecular basis of its interaction with Spindly. *J Cell Biol, 216*(4), 961-981.

Nicholas, M., Höök, P., Brenner, S., Wynne, C., Vallee, R., & Gennerich, A. (2015). Control of cytoplasmic dynein force production and processivity by its C-terminal domain. *Nature Communications, 6*(6206).

O'Connell, C., & Wang, Y. (2000, 5). Mammalian spindle orientation and position respond to changes in cell shape in a dynein-dependent fashion. *Molecular biology of the cell, 11*(5), 1765-1774.

Patel, S., Belmont, B., Sante, J., & Rexach, M. (2007). Natively Unfolded Nucleoporins Gate Protein Diffusion across the Nuclear Pore Complex. *Cell, 129*(1), 83-96.

Pereira, C., Reis, R., Gama, J., Celetino, R., Cheerambathur, D., Carvalho, A., & Gassmann, R. (2018). Self-Assembly of the RZZ Complex into Filaments Drives Kinetochore Expansion in the Absence of Microtubule Attachment. *Current Biology, 28*(5), 3408-3421.

Reck-Peterson, S., Yildiz, A., Carter, A., Gennerich, A., Zhang, N., & Vale, R. (2006). Single-molecule analysis of dynein processivity and stepping behavior. *Cell, 126*(2), 335-348.

Rieder CL, Cole RW, Khodjakov A, & Sluder G. (1995). The checkpoint delaying anaphase in response to chromosome monoorientation is mediated by an inhibitory signal produced by unattached kinetochores. *Journal of Cell Biology, 130*(4), 941-948.

Rodriguez-Rodriguez, J.-A., Lewis, C., McKinley, K., Sikirzhytski, V., Corona, J., Maciejowski, J., . . . Jallepalli, P. (2018). Distinct Roles of RZZ and Bub1-KNL1 in Mitotic Checkpoint Signaling and Kinetochore Expansion. *Current Biology, 28*(21), 3422-3429.

Sacristan, C., Ahmad, M., Keller, J., Fermie, J., Groenewold, V., Tromer, E., . . . Kops, G. (2018). Dynamic kinetochore size regulation promotes microtubule capture and chromosome biorientation in mitosis. *Nat Cell Biol, 20*, 800-810.

Sarangapani, K., & Asbury, C. (2014, 4). Catch and release: how do kinetochores hook the right microtubules during mitosis? *Trends in genetics : TIG, 30*(4), 150-159.

Schlager, M., Hoang, H., Urnavicius, L., Bullock, S., & Carter, A. (2014). In vitro reconstitution of a highly processive recombinant human dynein complex. *EMBO J, 33(17)*, 1845-1846.

Sladewski, T., Billington, N., Ali, Y., Bookwalter, C., Lu, H., Krementsova, E., . . . Trybus, K. (2018). Recruitment of two dyneins to an mRNA-dependent Bicaudal D transport complex. *eLife, e36306*.

Splinter, D., Razafsky, D., Schlager, M., Serra-Marques, A., Grigoriev, I., Demmers, J., . . . Akhmanova, A. (2012). BICD2, dynactin, and LIS1 cooperate in regulating dynein recruitment to cellular structures. *Mol Biol Cell, 23*(21), 4226-4241.

Stevens, D., Gassmann, R., Oegema, K., & Desai, A. (2011). Uncoordinated Loss of Chromatid Cohesion Is a Common Outcome of Extended Metaphase Arrest. *PLOS ONE, 6*(8).

Sukdakin, V., Ganoth, D., Dahan, A., Heller, H., Hershko, J., Luca, F., . . . Hershko, A. (1995). The cyclosome, a large complex containing cyclin-selective ubiquitin ligase activity, targets cyclins for destruction at the end of mitosis. *Molecular Biology of the Cell, 6*(2), 197.

Thompson, S., & Compton, D. (2010). Chromosomes and cancer cells. *Chromosome Research, 19*(3), 433-444.

Urnavicius, L., Zhang, K., Diamant, A., Motz, C., Schlager, M., Yu, M., . . . Carter, A. (2015). The structure of the dynactin complex and its interaction with dynein. *Science, 347*(6229), 1441-1446.

Varma, D., Monzo, P., Stehman, S., & Vallee, R. (2008, 9 22). Direct role of dynein motor in stable kinetochore-microtubule attachment, orientation, and alignment. *The Journal of cell biology, 182*(6), 1045-1054.

Visintin, R., Prinz, S., & Amon, A. (2007). CDC20 and CDH1: a family of substrate-specific activators of APC-dependent proteolysis. *Science, 278*(5337), 463.

Vleugel, M., Hoogendoorn, E., Snel, B., & Kops, G. (2012). Evolution and Function of the Mitotic Checkpoint. *Developmental Cell, 23*(2), 239-250.

Woodruff, J., Ferreira Gomes, B., Widlund, P., Mahamid, J., Honigmann, A., & Hyman, A. (2017). The Centrosome Is a Selective Condensate that Nucleates Microtubules by Concentrating Tubulin. *Cell, 169*(6), 1066-1077.e10.